ELSEVIER

Journal of Atmospheric and Solar-Terrestrial Physics 69 (2007) 191–211

Journal of ATMOSPHERIC AND SOLAR-TERRESTRIAL PHYSICS

www.elsevier.com/locate/jastp

The magnetosphere–ionosphere system from the perspective of plasma circulation: A tutorial

W. Lotko*

Thayer School of Engineering, Dartmouth College, Hanover, NH 03755-8000, USA

Received 1 May 2006; received in revised form 9 August 2006; accepted 10 August 2006
Available online 15 December 2006

Abstract

This tutorial review examines the role of O^+ in the dynamics of magnetosphere–ionosphere coupling. The life cycle of an O^+ plasma element is considered as it circulates from the mid- to high-latitude ionosphere. Energization and diversion of the convecting plasma element into outflows involves Alfvénic turbulence at the low-altitude base of the cusp and plasmasheet boundary layer and in downward-current "pressure cookers." Observational evidence indicating that O^+ dominates the plasmasheet and ring current during extreme storm intervals is reviewed. The impacts of an O^+-enriched plasma on solar wind–magnetosphere–ionosphere coupling are considered at both the micro and global scales. A synthesis of results from observation, theory and simulations suggests that the presence of O^+ in the magnetosphere is both a disruptive and a moderating agent in maintaining the balance between dayside and nightside magnetic merging.

Keywords: Magnetosphere–ionosphere interactions; Plasma redistribution; Ionospheric outflow; Storm dynamics

1. Introduction

It is difficult to imagine another pathway to convection that could lead to greater complexity or richer plasma dynamics of the coupled magnetosphere–ionosphere system than the phenomenon of magnetic reconnection. For four decades, this paradigm has generated theories and controversies for where and when reconnection should occur, why the episodic signatures and processes of reconnection in the magnetotail are so different from those at the dayside, and how the ionosphere regulates reconnection and convection. The scale of reconnection and its impacts on magnetospheric-ionospheric plasma circulation have also challenged observations at both extremes—global and micro. This tutorial will examine the interplay between magnetospheric and ionospheric plasma electrodynamics at these physical extremes. To be sure, observational progress has been steady (cf. Johnson, 1983; Shelley and Collin, 1991; Yau and André, 1997; Hultqvist et al., 1999; Huddleston et al., 2005), and the role of theory and computer simulation in advancing our understanding of magnetosphere–ionosphere system dynamics and plasma circulation has been indispensable.

We know that the motional electric field of the solar wind imposes a voltage across solar-wind connected, polar field lines (Reiff and Luhmann, 1986), and simple electrical considerations tell us

*Tel.: +1 603 646 3485; fax: +1 603 646 3856.
E-mail address: wlotko@dartmouth.edu.

1364-6826/$ - see front matter © 2006 Elsevier Ltd. All rights reserved.
doi:10.1016/j.jastp.2006.08.011

that the conductivity of the high-latitude ionosphere should regulate the dayside region 1 currents generated by this dynamo action. However, only recently have we recognized that these currents can significantly modify the geometry of the magnetopause, the magnetosheath flow around it and, consequently, the rate at which interplanetary magnetic flux is delivered to the magnetosphere (Merkine et al., 2003; Siscoe et al., 2004). This *electrodynamic feedback* limits the dynamo efficiency, particularly for the strongly driven stormtime system, and it explains in part why the magnetosphere–ionosphere system operates at only a fraction of the power available to it from the solar wind dynamo (Fedder and Lyon, 1987). What exactly determines the fractional rate of power transfer from the solar wind to the magnetosphere, for given ambient conditions, is an important global problem in solar wind—magnetosphere coupling that cannot be understood without consideration of the influence of the ionosphere in this coupling.

Our understanding of *inertial feedback* between the magnetosphere and ionosphere is presently in a far murkier state. It is well known that the high-latitude ionosphere is a persistent source of outflowing plasma and essentially the only source of singly ionized oxygen in the magnetosphere (Yau and André, 1997; Chappell et al., 2000). But are there implications of populating the magnetosphere with ionospheric O^+ that result in fundamentally different system dynamics? Is magnetospheric structure sensitive to the relative rates of supply and distribution of plasma from the solar wind and the ionosphere, or to the mass composition of the magnetosphere? Observation has revealed that the ionosphere does release enormous fluxes of O^+ during active periods, and it is known that ionospheric O^+ can dominate the plasma sheet (Peterson et al., 1981) and ring current (Lennartsson and Sharp, 1982) during such periods. The more recent observations to be considered here focus on the relationship between the mass composition of these regions and storm and substorm dynamics (Kistler et al., 2005; Nosé et al., 2005), especially for extreme events. New insights into the *electrodynamic* coupling between the solar wind, magnetosphere and ionosphere have emerged from investigations of the integrated system during storm intervals (Ober et al., 2003), and we might therefore expect to improve our understanding of *inertial* coupling and feedback in the solar wind–magnetosphere–ionosphere system by also focusing on such periods.

This descriptive overview examines some basic aspects of ionospheric plasma transport and energization, their implications for an upward exodus of ionospheric plasma, and the fate of the outflowing ionospheric plasma in the magnetosphere. The organizing perspective is the life cycle of an ionospheric O^+ plasma element as it convects from the midlatitude, dayside ionosphere through the dayside "convection throat", across the polar cap, into the nightside auroral zone, eventually merging into the sunward return flow. Along the ionospheric convection path, the plasma content of the element is progressively diminished through diversion of the convective transport into upward, field-aligned flows. Upon escaping gravity through processes that remain poorly understood, the liberated and energized O^+ ions join the magnetosphere circulation, but their presence seemingly has the capacity to undermine the dayside–nightside balance of magnetic flux transport. The impact of O^+ ionospheric outflow on solar wind–magnetosphere–ionosphere system dynamics is considered, although, as suggested above, the discussion here is somewhat tentative.

2. Surges in ionospheric plasma transport

Storm-enhanced transport of ionospheric plasma to high-latitudes is a consequence of at least two coincident conditions: (1) an inflated mid-latitude *F* region caused by the penetration of stormtime electric fields at low latitudes (Kelley et al., 2004); and (2) enhanced convection and entrainment of the mid-latitude dayside ionosphere in the polar circulation pattern (Foster et al., 2004). These conditions produce a plasma convective surge that flows toward the dayside convection throat from mid-latitudes. The phenomenon may be observationally visualized by projecting "instantaneous" maps of total electron content (TEC) derived from ground GPS receivers onto a "simultaneous" snapshot of the global convection pattern inferred from SuperDARN measurements (Foster et al., 2005). Fig. 1 shows such a surge, or "tongue of ionization" (Sato, 1959; Sojka et al., 1993), 2 h after its leading edge first entered the dayside cusp, nominally located at 70–75° latitude. It carries 10^{26} ions/s from the mid-latitude ionosphere into the convection throat (Foster et al., 2004). The TEC increase in the cusp, and/or immediately poleward of it, is due in part to the precipitation of soft magnetosheath electrons (Knudsen, 1974).

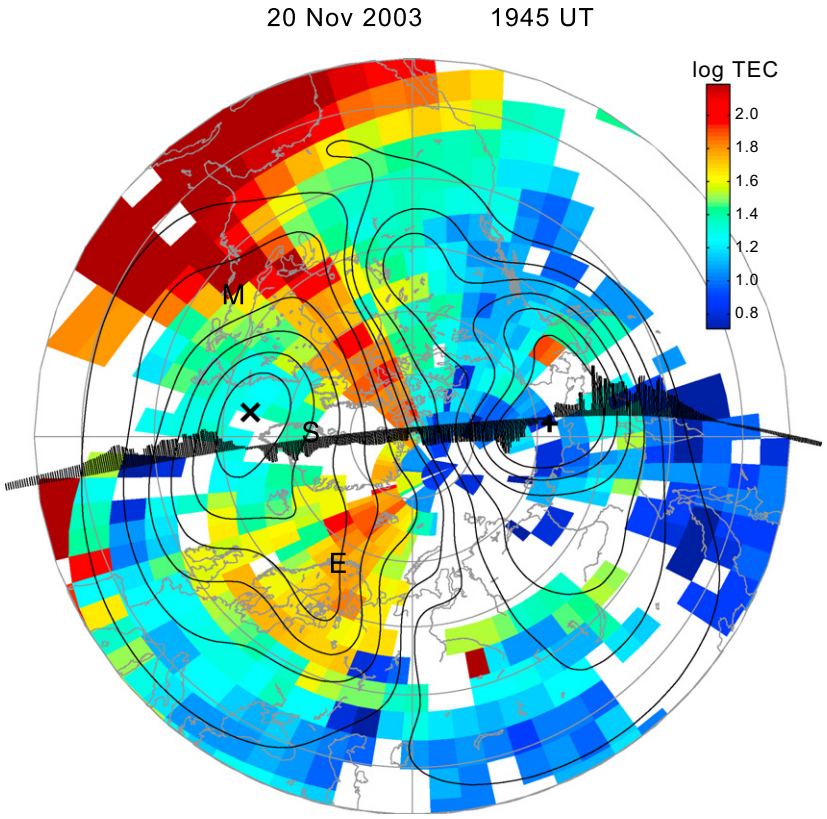

Fig. 1. Vertical GPS TEC observations binned by latitude and longitude at 350 km altitude are displayed with the temporally overlapping cross-track velocity from the DMSP F-13 drift meter and the convection pattern derived from SuperDARN radars. A polar geomagnetic grid is overlaid with 10° latitude circles, above 60° latitude with noon at the top. A large geospace storm with *Dst* reaching −500 nT is in progress. The tongue of ionization plume extends continuously from its low-latitude source in the prenoon sector, through the dayside cusp and across the polar cap to the midnight sector (from Foster et al., 2005).

The TEC values are seen to be largest in the mid-latitude dayside region and progressively decrease, with some variability, along the convective path as the plasma moves across the polar cap from dayside to nightside. The weak antisunward gradient in TEC over the polar cap may arise from the divergence of streamlines evident in Fig. 1. Plasma diffusion enhanced by gradient–drift instabilities (e.g., Sojka et al., 1998) may also play a role, but because diffusion is most effective at steep gradients, the fast convection appears to maintain the integrity of the large-scale surge as it traverses the polar cap.

The topside plasma density decreases in and poleward of the cusp where the convecting *F*-region plasma is diverted into field-aligned outflows, as described in more detail below. Note that these outflows continue to contribute to the TEC until they reach several R_E altitude, at which point they are above the line of sight of the GPS satellites used to infer TEC. Thus the reduction in the topside density is not as evident in the TEC maps as in incoherent scatter radar data (Foster et al., 2005).

The character of the outflow, and the energization that enables O^+ to overcome gravity, varies along the convection path. The dayside cusp and the nightside auroral-polar cap boundary regions corresponding, respectively, to the low-altitude projections of dayside and nightside reconnection activity exhibit intense Alfvén-wave turbulence, ion transverse heating and upward field-aligned ion flows. At higher latitudes, a thermal polar wind expands into the low-pressure lobe from the polar cap (Banks and Holzer, 1968). The stormtime polar wind exhibits considerable structure in space and time (Schunk and Sojka, 1997) and can be dominated by O^+ (Yau and André, 1997), in contrast with the non-stormtime polar wind which, statistically, is an H^+ polar wind, at least near solar minimum. At solar maximum an elevated topside density resulting

from enhanced solar EUV fluxes sustains larger O^+ thermal outflows relative to the solar-minimum average (Cannata and Gombosi, 1989; Abe et al., 2004), much more so than the relative increase in H^+ outflow from solar minimum to maximum, thus resulting in higher concentrations of O^+ in the polar wind at solar-maximum (Cully et al., 2003). The processes responsible for producing the polar wind are actually present at essentially all latitudes, including those in and equatorward of the auroral zone; however, the associated outflow is substantially modified from the "classic polar wind" at nonpolar latitudes by wave–particle interactions and outflow-limiting boundary conditions.

The plasma tongue shown in Fig. 1 upwells again relative to its polar cap signature as it drifts into the nightside auroral zone where Joule heating and soft electron precipitation are enhanced relative to their rates in the polar cap. Some of the ions are energized by parallel electric fields and become upward field-aligned ion beams in regions of upward field-aligned current and inverted-V electron precipitation. As the now more strongly diverging plasma elements of the tongue move into the low-latitude portion of the premidnight auroral oval and turn sunward, they enter a zone of downward-directed field-aligned current, i.e., the duskside region-2 current. Time-dependent, downward-directed, field-aligned electric fields exist in such regions (Carlson et al., 1998; Andersson et al., 2002), as well as in smaller scale, return current regions associated with auroral arcs. These regions give rise to the so-called pressure cooker effect (Gorney et al., 1985), which also produces large outflows.

Of the various processes and low-altitude regions where ions are accelerated to superthermal escape velocities, the outflowing number flux tends to be smallest in the inverted-V precipitation regions (more on this claim in the next section). The quiet time and active polar wind can be a significant source of outflowing thermal plasma. The physics of outflows in inverted V regions and the polar wind have been studied extensively and will not be considered in detail here. The next section focuses on the processes of superthermal ion energization and outflow in the cusp and auroral-polar cap boundary regions and the downward current region. By most estimates, these three regions produce the bulk of the O^+ that reaches the magnetosphere. All three are characterized by intense Alfvénic activity of different origins, with important consequences for magnetosphere–ionosphere coupling.

Table 1
Statistical outflow fluences by process and region, in units of 10^{25} ions/s[a]

	Quiet (Kp = 0–2)		Active (Kp = 3–5)	
	H^+	O^+	H^+	O^+
Polar wind (*solar max*)				
Polar cap	0.9–1.1	0.5–0.7	0.6–0.8	0.6–0.7
Auroral	1.8–2.6	0.8–1.2	3.5–4.0	1.5–2.2
Upwelling ions (*solar max*)				
Cleft	~0.5	~2.0	~0.5	~2.0
Upflowing ions (*solar max*)				
Polar cap	0.3–0.5	0.3–1.0	1.2–1.8	3.0–6.0
Auroral	2.0–3.1	1.2–4.1	3.9–6.2	7.0–14.0
Upflowing ions (*solar min*)				
Polar cap	0.5–0.8	0.1–0.3	1.6–2.6	0.7–2.7
Auroral	1.8–2.8	0.4–0.9	3.4–5.5	1.3–3.6

[a]From Yau and André (1997).

To put the above claim in context, the statistical classification of ion outflows developed by Yau and André (1997) is duplicated here as Table 1. A revised version of the table and its classification scheme should probably be undertaken in light of the many subsequent and relevant results derived from the Akebono (Cully et al., 2003; Abe et al., 2004), FAST (Andersson et al., 2005), Polar (Peterson et al., 2001, 2006; Lennartsson et al., 2004), and Geotail, Interball and Cluster (Bouhram et al., 2004; Nilsson et al., 2006) satellites. In particular, Yau and Andre's superthermal "upwelling" population in the cleft may be mainly the low-altitude and/or low-energy signature of what they identify as "upflowing ions" in the polar cap, both being a consequence of ion energization and outflow from the low-altitude cusp region. Yau and Andre's auroral polar wind may also become their auroral "upflowing ions" if the auroral polar wind ions are energized above the altitude where they are identified as a polar wind. If such reclassifications are appropriate, they indicate that the cusp and auroral outflows are the dominant source of ionospheric plasma, especially O^+ ions, flowing into the magnetosphere.

3. Alfvénic energization and outflow

The production of intense fluxes of outflowing superthermal ions requires two primary ingredients: (1) a high-density topside source plasma, which may be produced in several different ways as described

below; and (2) a source of electromagnetic power cascading to the extreme low-frequency regime where efficient wave-ion energy transfer occurs (Lund et al., 2000). This power flows as a Poynting flux along geomagnetic field lines from magnetospheric dynamo regions. The optimum altitude for production of intense outflows is not known precisely and may vary with the particular wave–particle interactions involved. Most of the microscopic wave–particle interactions that produce transversely accelerated ions break the first adiabatic invariant. Because the ion gyroradius and gyroperiod increase with altitude, the mechanisms that produce transverse ion acceleration prefer relatively high altitudes. However, if the altitude of the energization region is too high, few ions will be energized because the density of the ionospheric source plasma decreases with altitude and will be relatively low. Variations in wave propagation characteristics with ambient properties also complicate an assessment of the optimum altitude for energization. After attaining sufficient perpendicular energy, the transversely accelerated ions are propelled upward by the mirror force and escape into the magnetosphere.

From a systems perspective, the causal relationships between electromagnetic power flowing into a low-altitude energization region and the properties of the superthermal ion fluxes flowing upward from it are not very well characterized. For example, we do not yet know how to specify, in general terms, the rate of outflow for given input power. A comparison between empirical studies based on FAST (Strangeway et al., 2005) and Polar (Zheng et al., 2005) satellite data suggest that such relationships may be quite complicated, with hidden or untested variables modifying the relation for different ambient conditions. The transport law undoubtedly depends on both the frequency and wavenumber spectra of the power source and the initial density, stratification, composition and energy of the source plasma. Both DC and time-variable electromagnetic power flows are relevant, but the associated pathways to ion energization can be very different. Two different processes will be discussed here: (1) energization in cusp and auroral-polar cap boundary regions wherein the AC Poynting flux transmitted from the magnetosphere by Alfvén waves is the primary agent; and (2) energization in downward current regions sustained by DC Poynting fluxes on the large scale; these regions eventually break-up into filamentary currents of feedback-unstable, ionospheric Alfvén resonator modes.

The flowchart developed by Strangeway et al. (2005) to illustrate the interrelationships between the various processes leading to cusp-region ion outflow builds on a large body of previous work and identifies two primary causes of *F*-region upwelling: (1) ion frictional heating in the *E* and lower *F* layers due to enhanced convection, wherein bottomside heating increases the upward ion pressure gradient, thereby causing upwelling; and (2) an upward ambipolar electric field in regions of enhanced soft ($\sim$100 eV) electron precipitation, e.g., in the cusp and nightside Alfvénic regions. Soft electron precipitation deposits energy in the *F* region, increases the upward electron pressure gradient there, and, through the ambipolar field, forces the *F*-region ions upward, again causing upwelling. Modeling studies (Liu et al., 1995) indicate that soft electron precipitation is usually more effective in producing upwelling than Joule heating. The TEC-convection map in Fig. 1 and supporting analysis by Foster et al. (2005) suggest an important third way of swelling the topside ion density in the cusp energization region, also in the nightside auroral-polar cap boundary region: convection of a parcel of inflated topside ionosphere into the energization region from another region of the ionosphere.

Fig. 2 adapted from Zheng et al. (2005) shows in situ measurements in an energization region near 1 R_E altitude above the magnetic footpoint of the cusp. The signature of the cusp is evident in the enhanced ion and electron fluxes from 1624 to 1628 UT. The outflow flux for this event exceeds 10^{12} ions/m^2 s (third panel down), during a period of moderate geomagnetic activity (*Kp* 3). According to Zheng et al. the outflowing ion flux is dominated by O^+. It correlates well with the soft electron precipitation in the bottom panel and with the field-aligned, downgoing Poynting flux, bandpass filtered at 1/600–1/6 Hz. This event is typical of low-altitude cusp-region outflow, which is always a significant source of O^+, especially during storm times and during the passage of coronal mass ejections past earth (Moore et al., 1999). The cusp also continues to be an important though not dominant source of outflowing O^+ during nonstorm periods (Peterson et al., 2006).

As the ions stream upward along antisunward convecting magnetic field lines typical of southward IMF conditions, the resulting dispersion of the outflow, with higher energy ions reaching higher

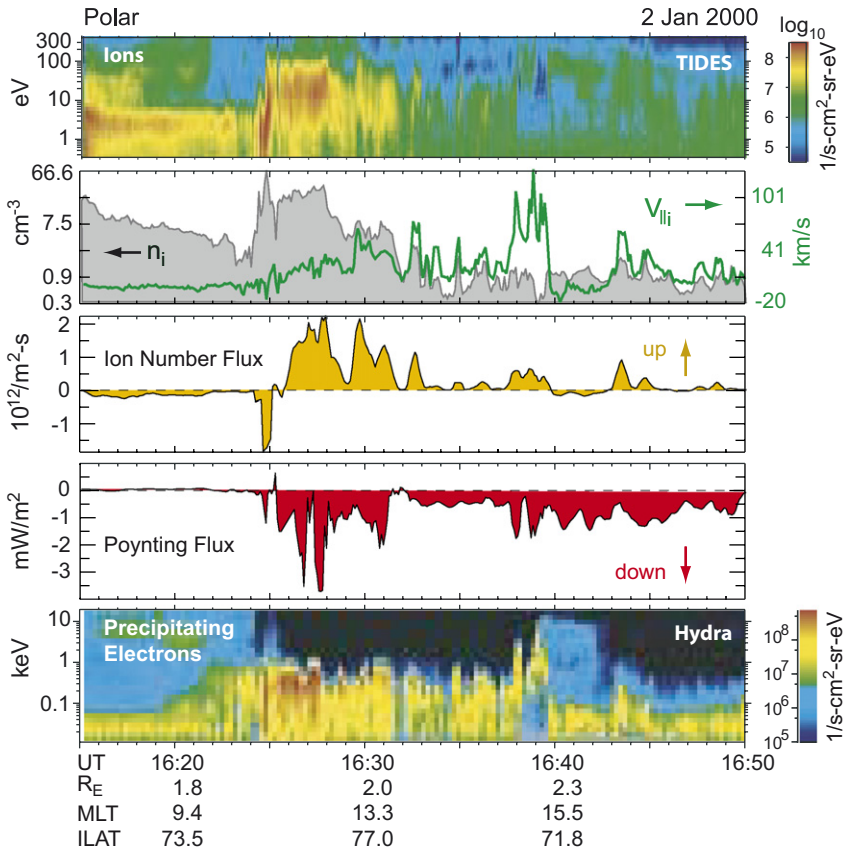

Fig. 2. Polar satellite pass through the cusp region at an altitude near 1 R_E showing the relationship between ion outflow flux (primarily O^+), downward Poynting flux and electron precipitation (adapted from Zheng et al., 2005).

altitude at lower latitudes (sunward of the pole), has been termed the cusp or cleft "ion fountain" (Lockwood et al., 1985). The ion fountain is a permanent feature of dayside outflows, although, as the variation in ion number flux in Fig. 2 attests, it never achieves steady-state conditions (Bouhram et al., 2004). The persistent enhanced Poynting fluxes flowing into the low-altitude cusp region from the magnetosphere are almost certainly stimulated by variability at the magnetopause, including boundary disturbances attributed to time-dependent reconnection and upstream pressure and IMF variations. Direct access of ULF waves into the cusp may also contribute to the field-aligned Poynting flux flowing to low altitude. This variability coupled with variable convection and soft electron precipitation and structure in the topside ion source all contribute to the non-stationarity of the cusp-region outflows observed at higher altitudes.

The ion outflow and energization depicted in Fig. 2 actually represents only a slice of the larger picture. Combined observations from FAST and Akebono below 1.6 R_E altitude, from Interball 2 at 1.5–3 R_E altitude, and from Cluster at altitudes $>3.5\,R_E$ in the cusp/cleft region indicate that the cusp/cleft ion fountain is heated continuously up to an altitude of about 3.5 R_E and attains maximum energies of a few keV (Bouhram et al., 2004). This 3.5 R_E high heating zone, straddling cusp field lines and spanning 1–2° of invariant magnetic latitude, has been termed the polar cusp "heating wall" (Knudsen et al., 1994). For all IMF orientations, the outflow evidently starts on average about 1.5° equatorward of the low-latitude edge of the cusp, where the parallel and perpendicular temperatures are observed to be elevated by a factor of 3 relative to those at the higher-latitude edge of the cusp (Valek et al., 2002). This cleft region outflow is connected with mode conversion of surface waves

into kinetic Alfvén waves in the low-latitude boundary layer, with attendant ion heating at lower altitudes (Chaston et al., 2005).

Returning to the picture of storm-enhanced convection depicted in Fig. 1, it seems imminently plausible that as the swelled topside ionosphere convects into the cusp from lower latitudes, the electromagnetic power already flowing into the cusp-region ionosphere from high altitude will energize the underlying convecting plasma, thereby augmenting any pre-existing outflow in the cusp. This causal scenario has not yet been recorded in an event study on the dayside. However, the data shown in Fig. 3 demonstrate that it has clearly been seen on the nightside (Semeter et al., 2003).

The bottom portion of Fig. 3 shows 5 min of vertical scans from the Sondrestrom incoherent scatter radar with the three panels from bottom up showing upward ion number flux (F_i), upward ion velocity (V_i) and plasma density (N_e) as functions of altitude and UT. The large *F*-region density "patch" evident between 23:29:30 and 23:30:30 UT convected from the premidnight polar cap into the field of view of the ISR, at a time when the polar cap boundary was above the radar. The patch subsequently drifted to lower latitudes into the auroral zone.

The 1 min averages of the plasma density, upward ion velocity and upward number flux versus altitude shown in the top panels were recorded just before, during and after the patch drifted through the field of view. The upward ion velocity in the topside *F* region was enhanced throughout the entire interval and did not change substantially during the

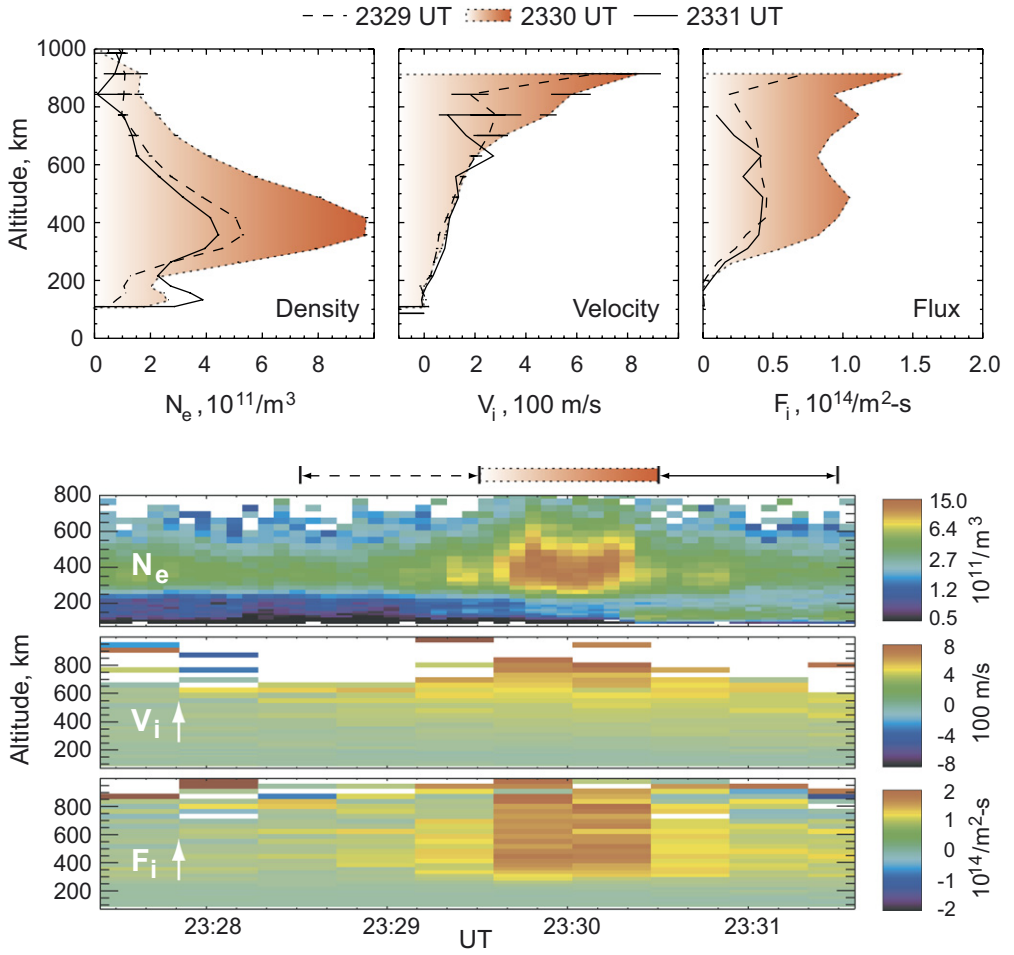

Fig. 3. Sondrestrom incoherent scatter radar measurements of upward ion flux (F_i), velocity (V_i) and electron density (N_e) during the overhead passage of a polar plasma patch drifting from the polar cap into the nightside auroral zone. Plots in upper panels are one-minute averages over intervals indicated in lower panels (adapted from Semeter et al., 2003).

encounter with the patch (upper middle plot), while the number density and upward number flux essentially doubled when the patch was within the ISR field of view. This event provides compelling evidence for the concept of a magnetospherically powered, spatially locked energization region, with the underlying ionospheric source population convecting through it, thereby enhancing the magnetosphere's uptake of ionospheric plasma. It is reasonable to assume that this process also operates in the cusp region.

This causal sequence is distinct from the dynamic process reported by Carlson et al. (2006), wherein transient dayside reconnection causes an equatorward leap of the dayside plasma flow boundary, which "captures" a parcel of subauroral plasma that subsequently flows directly into the polar cap, creating a locally enhanced (primarily H^+) polar wind or propagating polar jet above its convective trajectory (Schunk et al., 2005).

While the low-altitude cusp and cleft regions are the most persistent sources of magnetospheric O^+, accounting for about 1/3 of the total O^+ outflow during quiet times at solar minimum (Peterson et al., 2006), the nightside auroral region produces the most energetic and largest peak fluxes of O^+ outflows during active periods (Tung et al., 2001). The event shown in Fig. 4 (adapted from Paschmann et al., 2003) illustrates the morphology of nightside auroral outflows and their relation to electron characteristics, field-aligned current and low-frequency turbulence. From top to bottom, the figure shows the east-west magnetic and north–south electric fields, electron energy and pitch angle distributions and upflowing ion flux recorded by the FAST satellite in the premidnight auroral sector. Consider the time sequence from the perspective of the underlying ionospheric plasma entrained in the high-latitude convection, e.g., Fig. 1. Reading Fig. 4 from *right to left*, our *F*-region plasma parcel exits the polar cap (the quiescent dark region in the electron distributions in Fig. 4), and immediately enters a region of intense Alfvén wave activity (evident in E_{NS}), corresponding to the low-altitude projection of the plasmasheet boundary layer. This particular satellite pass over the northern auroral zone occurred during a substorm. The ion outflow flux in this region exceeds 10^{12} ions/m^2 s.

This region of Alfvén wave activity is the nightside version of cusp-region Alfvénic activity.

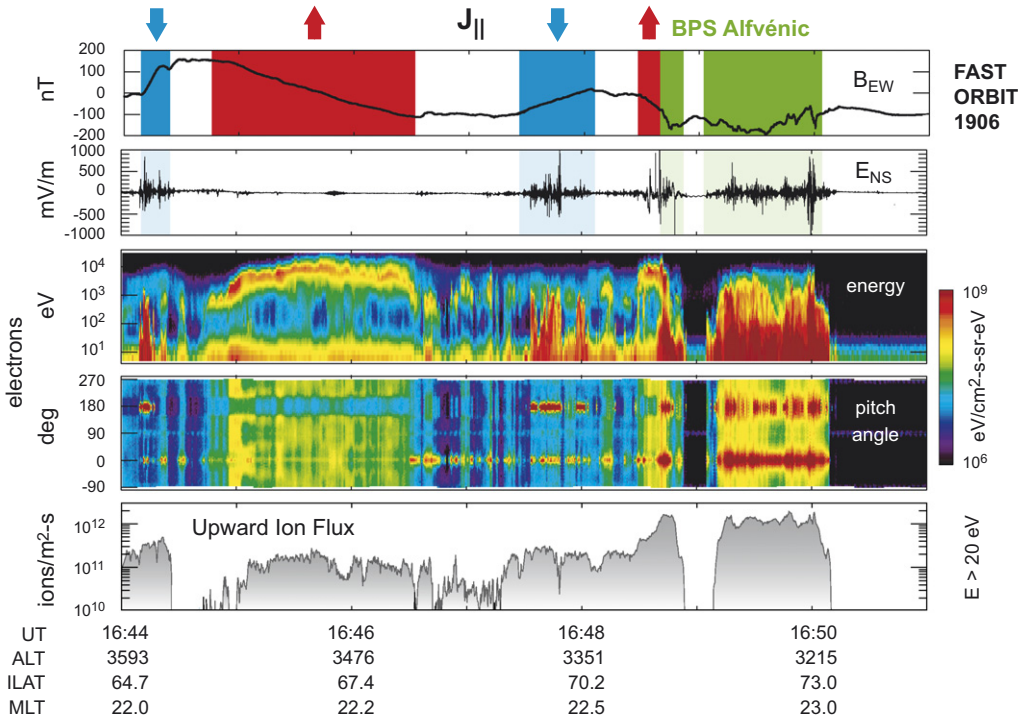

Fig. 4. FAST satellite pass on 13 February 1997 across the premidnight northern auroral zone at an altitude of about $\frac{1}{2}R_E$ showing three characteristic acceleration regions: (1) Alfvénic boundary plasma sheet just equatorward of the polar cap boundary, (2) upward field-aligned current (inverted-V) regions, and (3) downward field-aligned current regions (adapted from Paschmann et al., 2003).

Keiling et al. (2003) have shown that the cusp and premidnight boundary plasma sheet regions statistically are the principal sites of intense Alfvénic Poynting fluxes (left panel of Fig. 5). Their analysis of two years of Polar satellite data of electromagnetic fluctuations in the passband from 6 to 180 s indicates that, on average, Alfvénic power transmitted to altitudes below the Polar satellite is substantially absorbed. FAST particle data obtained at altitudes below Polar indicates that power in this passband is absorbed primarily by electrons, which creates the intense field-aligned fluxes of superthermal electrons (Chaston et al., 2003; Dombeck et al., 2005) evident in the region of Alfvénic activity in Fig. 4. Some of the Alfvénic power is also absorbed by transversely accelerated ions (TAIs), producing keV ions at FAST altitudes (Chaston et al., 2004). As in the cusp regions, the action of the mirror force on the TAIs produces the observed ion outflows.

The statistical pattern of intense Alfvénic activity in Fig. 5 exhibits some similarities to the observed statistical pattern in the number flux of outflowing O^+ (right panel of Fig. 5) derived from Polar-satellite perigee passes near 1-R_E altitude by Lennartsson et al. (2004). The regions of greatest Alfvénic activity and O^+ outflow occur in approximately the same local time sectors, but the latitudes of the most intense outflows in the premidnight sector occur at lower latitudes than those of the intense Alfvénic activity. Some of the differences in the patterns of Poynting and O^+ fluxes may be due to (a) different sampling periods for the data, (b) different altitudes of measurement, and (c) different binning and magnetic mapping procedures. The lower latitude of intense premidnight O^+ fluxes relative to that of intense Poynting fluxes may also be caused by persistent outflows from "pressure cookers" in the region-2 downward currents as described below. A statistical study based on the lower altitude FAST data is consistent with the conclusion that the greatest fluxes of outflowing O^+ occur near the polar cap boundary, but the characteristic energy of the O^+ outflow is largest near the equatorward boundary, especially in the midnight sector (Andersson et al., 2005). The variation in characteristic energy across the auroral oval is undoubtedly due to the different energization processes operating in different regions as discussed below. Not surprisingly, the observed statistical pattern of dc Poynting fluxes flowing to low altitude reported by Gary et al. (1995) and Olsson et al. (2004) does not correlate as well with the regions of intense outflows, particularly on the nightside. The

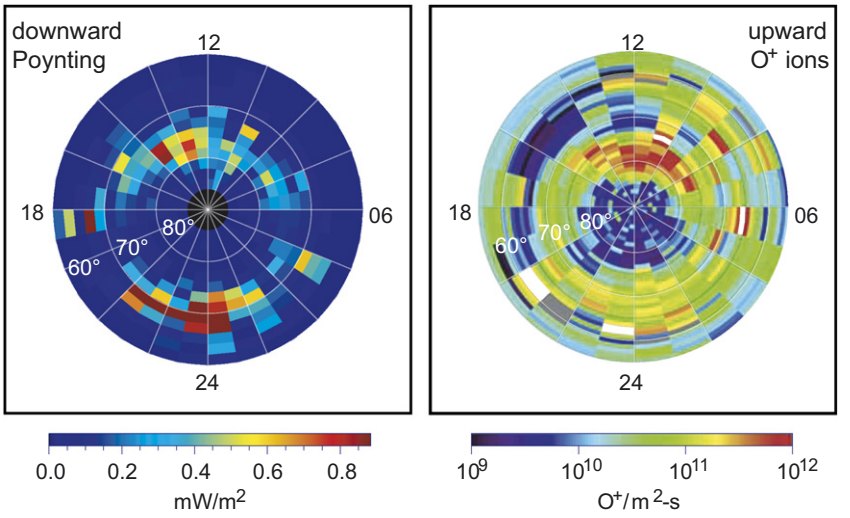

Fig. 5. Statistical patterns of magnetic field-aligned Poynting flux (left) in the passband from 6 to 180 s flowing toward the ionosphere (adapted with permission from Keiling et al., The global morphology of wave Poynting flux: powering the aurora. Science 299, 383–386. Copyright 2003 AAAS) and magnetic field-aligned number flux of O^+ ions (right) streaming away from the ionosphere (adapted from Lennartsson et al., 2004), both from the Polar satellite. The Poynting fluxes were measured at altitudes of 25,000–38,000 km over the northern hemisphere from January to December, 1997, are averaged over a 30 s sliding interval, and are projected along IGRF field lines to a common reference altitude of 100 km. The O^+ data are from southern perigee passes near 1 R_E altitude obtained from October 1997 to March 1998, the binning is done with the eccentric dipole EDMLT and ILAT supplied with the Polar satellite ephemeris, and the O^+ fluxes are projected to a common reference altitude of 300 km. White bins in the right plot are saturated; gray bins have no data.

most intense dc Poynting fluxes occur in regions where the dayside region 1 currents are diverted via Pedersen currents into the dayside region 2 currents. Upwelling occurs in such regions but not necessarily outflow.

Returning now to Fig. 4 and continuing from *right to left* from the Alfvénic BPS region, a relatively narrow, probably substorm-induced, pair of field-aligned currents, upward then downward, is encountered. A larger-scale system of up-then-down currents, characteristic of the region 1/2 currents of Iijima and Potemra (1976), occurs equatorward of the narrower current pair. This auroral crossing suggests that regions of downward field-aligned current sustain the second largest fluxes of auroral ion outflows, approaching 5×10^{11} ions/m^2 s for this event, after the BPS region of Alfvénic activity and greater than the outflowing ion flux in regions of upward field-aligned current. This same relative ordering of the magnitude of outflow flux is expected to persist at higher altitudes. The quasi-static, upward-directed, parallel electric fields that occur in regions of upward field-aligned current (inverted V precipitation regions) to first order preserve the field-aligned ion flux while adiabatically boosting the ion beam energy.

The large outflows in the downward current regions are created through the action of an "ion pressure cooker" (Gorney et al., 1985; Lynch et al., 2002), formed by downward parallel electric fields that retard the upward motion of the ions while the mirror force retards their downward motion. When the trapped ions are subjected to turbulent heating by the broadband extreme low-frequency (BBELF) fluctuations evident in the north–south electric field in the downward current regions in Fig. 4, they are steadily energized until the perpendicular energy of the ions is sufficiently large that the upward mirror force ($\propto -v_\perp^2 B \nabla B^{-1}$) exceeds the downward electrostatic retarding force. The striking coincidence in Fig. 4 of BBELF turbulence in nightside regions of downward current, with a relative paucity of turbulence in upward currents, begs for an explanation.

To understand the phenomenon, it is necessary first to consider the basic electrodynamics of MI coupling in up-down field-aligned current pairs. The right panel in Fig. 6 is a schematic adapted from a figure developed by Opgenoorth (in Paschmann et al., 2003) of the ionosphere where the field-aligned currents close as Pedersen currents in the *E* and lower *F* regions. In the upward current channel, the precipitating electrons increase the ionospheric conductivity. Since precipitating electrons in upward currents are usually energized to keV and larger by parallel electric fields near 1 R_E altitude, the enhancement in conductivity is significant because each precipitating energetic electron produces multiple ionizations. This enhanced conductivity shields (reduces) the perpendicular electric field in the ionospheric conducting layer, as required by Ohm's law and current continuity. In the adjacent downward current channel an upward exodus of electrons from the conducting layer is required to carry the downward current, while the ions in the conducting layer migrate across field lines to the upward current channel to neutralize the precipitating electrons. The net effect is a local

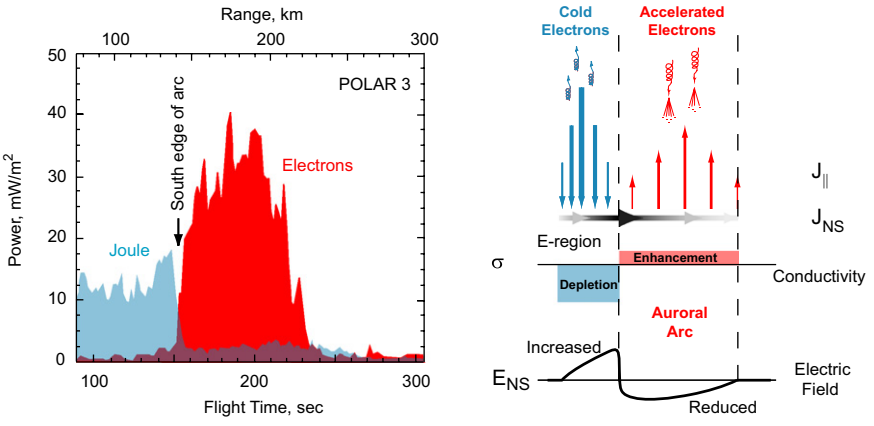

Fig. 6. Schematic of ionospheric electrodynamics (right) in an up-down current system (adapted from Paschmann et al., 2003) and measurements of electron energy flux and inferred ionospheric Joule dissipation (left) from the Polar 3 rocket experiment (adapted from Evans et al., 1977).

reduction in conductivity below the downward current, so that a larger perpendicular electric field is needed to drive the required Pedersen current in the downward current channel.

One immediate consequence of this situation is a partition of the field-aligned Poynting flux required to power the up-down current system. The Poynting flux is mostly converted to field-aligned electron energy at higher altitudes in the upward current channel. A larger fraction of the Poynting flux is required to power the more dissipative Pedersen current in the low-conductivity channel below the downward current. The rocket observation from Evans et al. (1977) shown in the left panel of Fig. 6 convincingly confirms this effect. The abrupt change in the combined energy flux across the up-down boundary in the Evans et al. data suggests that some of the downward-directed Poynting flux in the downward current channel is absorbed above the measurement altitude. The formation of downward parallel electric fields in downward current channels, and the attendant energy absorption that creates the upward accelerated, superthermal electrons evident in Fig. 4 in such regions, probably accounts for most of the difference.

The situation shown in Fig. 6 can never reach a true steady-state because the upward exodus of electrons in the downward current channel would eventually require an intolerably large electric field to maintain current continuity in the ionospheric conducting layer. The time scale for severe plasma depletion in the nightside ionosphere is on the order of 10 s (Doe et al., 1995).

The development of a low-conductivity, high-electric-field state of the conducting layer promotes the so-called feedback instability (Atkinson, 1970; Sato, 1978) of the ionospheric Alfvén resonator (Lysak and Song, 2002; Pokhotelov et al., 2002). This cavity resonator is bounded by the ionospheric conducting layer at low altitude; its lossy upper boundary is formed in part by the steep gradient in Alfvén speed at altitudes of 1–2 R_E. Apropos of the situation in downward current channels, a low-loss upper boundary is created by the effective resistivity of a downward-directed parallel electric field (Streltsov and Lotko, 2003).

Simulations of the nonlinear evolution of the feedback instability in up–down current pairs produce the filamentary field-aligned currents and intense BBELF electric field fluctuations, observed in the downward current regions in Fig. 4. Rubber-sheet representations of simulated $j_\parallel$ (left) and E_{NS} (right) are shown in Fig. 7 taken from Streltsov and Lotko (2004). The fiduciary $t = 0$ marks the time at which the large-scale up-down current pair is firmly established in this time-dependent simulation of Alfvén wave dynamics in dipole geometry. A simplified version of the active ionospheric model described by Doe et al. (1995) is included, together with magnetic field-aligned plasma inhomogeneity representative of nightside flux tubes bounded by $7.25 < L < 8.25$. At $t = 0$, the downward current, corresponding to the (right) downward deflection in the rubber-sheet plots of $j_\parallel$, starts draining the electrons in the simulated E-region. Feedback instability subsequently develops on a time scale of one minute when the first 10-km scale structure is well developed. As time proceeds, additional small-scale structure develops in both $j_\parallel$ and E_{NS}. These feedback-unstable resonator modes eventually fill the downward current channel and thwart continued drainage of the ionization required for the Pedersen current.

4. Ionospheric exodus and fate

The outflows discussed above contribute mass, momentum and energy to the magnetosphere. As discussed below, they can comprise the dominant population of the plasmasheet during storms when the outflow rate is high and convection is strongly enhanced. High time resolution measurements from the Cluster satellites have shown that H^+, He^+, and O^+ ions are injected into the tail during substorms from the nightside ionosphere, with a single injection accounting for over 80% of the oxygen population of the midtail plasmasheet during storms (Sauvaud et al., 2004). Inside the lobes, during disturbed times, ionospheric oxygen ions appear as quasi-field-aligned, nearly mono-energetic beams, propagating antisunward from the ionosphere (Sharp et al., 1981; Seki et al., 1998; Sauvaud et al., 2004). Coincident O^+ and H^+ beams with the same energy are sometimes observed, as well as beams in which all mass constituents move with approximately the velocity (Sharp et al., 1981). The former case may be associated with energization by parallel electric fields that give rise to mass-independent energization. The latter case is most likely associated with centrifugal acceleration (Cladis, 1986) of boundary layer and cleft ion fountain ions. Centrifugal acceleration ($\mathbf{v}_E \cdot d\mathbf{b}/dt$ with $\mathbf{b} = \mathbf{B}/B$) is independent of both mass and charge, so all species experiencing it will follow the

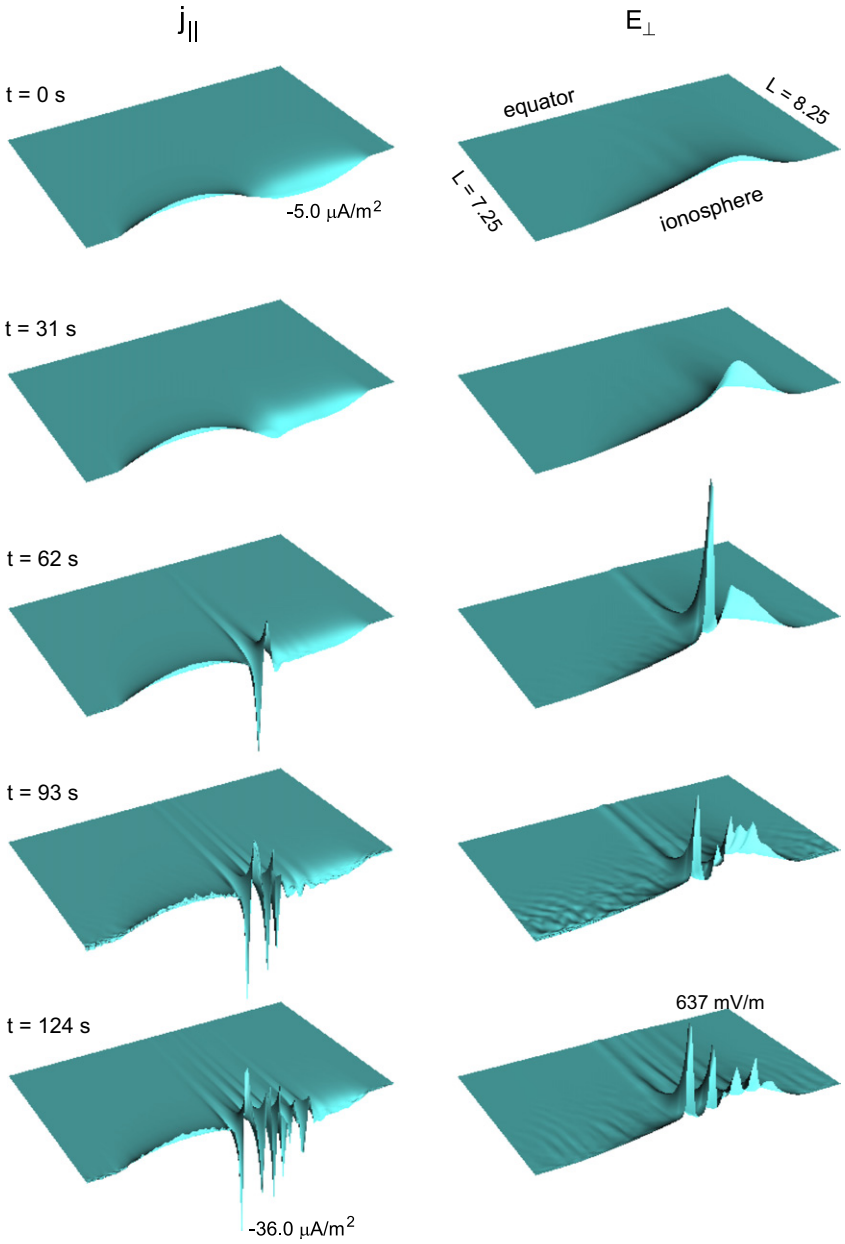

Fig. 7. Time sequence of rubber-sheet representations of the field-aligned current (left) and north-south electric field (right) obtained from a 2D, two-fluid MHD simulation in dipole magnetic geometry, including an active ionosphere. The simulation domain spans flux tubes from $7.25 < L < 8.25$, with a realistic density distribution from the E region to the magnetic equator. An up-down current pair like the one illustrated in Fig. 6 is evident in $j_{\|}$ at $t = 0$ with the up/down channel represented by the up/down deflection of the rubber sheet. The turbulence is produced by feedback-unstable ionospheric resonator modes (from Streltsov and Lotko, 2004).

same path in the magnetosphere and undergo the same acceleration, with an increase in parallel velocity by factors of 10–100 upon reaching the center plane of the magnetotail at distances greater than about $12\,R_E$ from the earth (Cladis et al., 2000). Upon encountering a thin magnetotail neutral sheet, energized ionospheric particles are subjected to nonadiabatic scattering and further acceleration in the cross-tail convection electric field.

Under normal conditions, the density of O^+ ions in the plasmasheet never exceeds that of protons;

however, they may contribute tens of percent to the total number and even approach the number density of H^+ near the centerline of the magnetotail (GSM $Y,Z \approx 0$) when the auroral electrojet index AE is large (Lennartsson and Shelley, 1986). For unusual conditions surrounding stormtime substorms, O^+ can actually dominate the both ion pressure and number density of the plasmasheet. Fig. 8 shows plasmasheet ion data for such an event (adapted from Kistler et al., 2005), a moderate storm characterized by a *Dst* minimum of −150 nT. The increase in plasma pressure during the substorm growth phase is punctuated by a peak at substorm onset at approximately 0927 UT, with a subsequent decrease in both pressure and the inferred half-width of the magnetotail current sheet to 10% of their growth phase values. The proton ion velocity is initially tailward indicating that the X-line was earthward of the spacecraft; V_x reverses at 0941 UT, becoming earthward, indicating that the X-line has migrated tailward of the spacecraft. About one minute after the V_x flow reversal in H^+, oxygen becomes the dominant plasmasheet ion. However, its density has not appreciably increased; rather the H^+ density is smaller on the earthward side of the X-line.

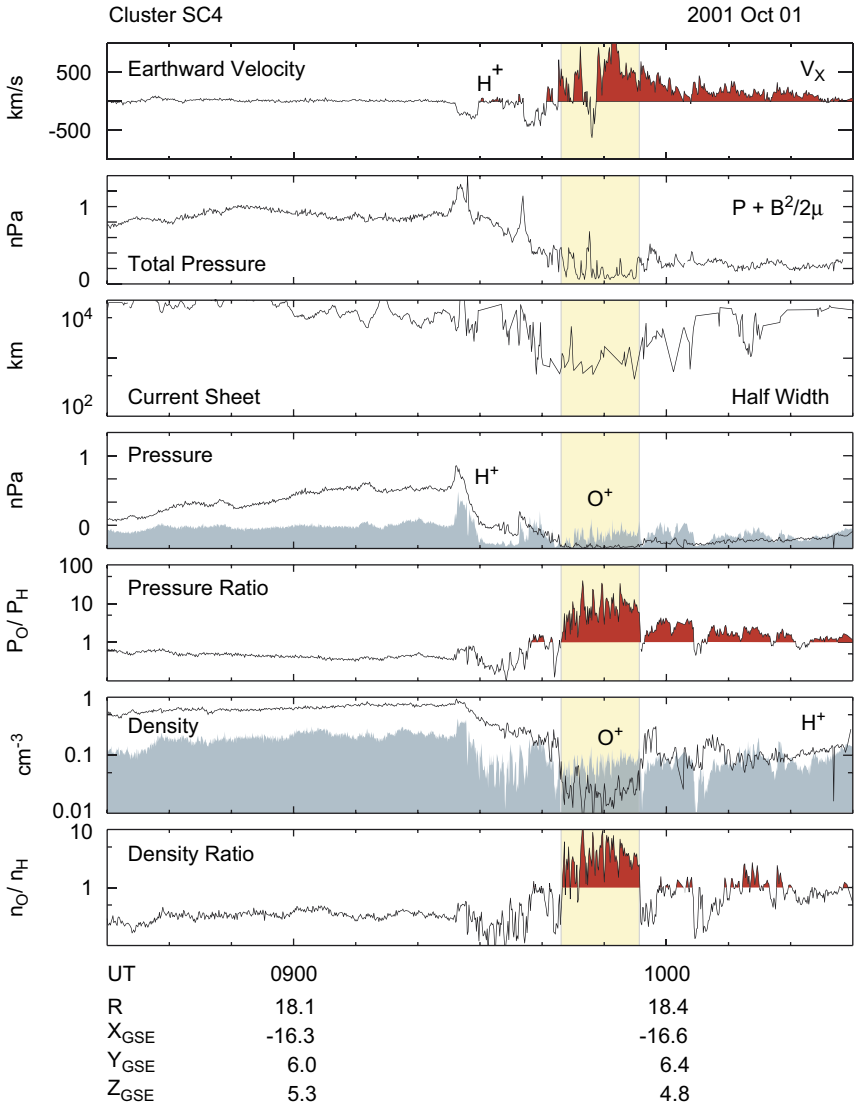

Fig. 8. Cluster satellite traversal of the plasmasheet during a stormtime substorm. The plasmasheet density and pressure are dominated by O^+ during the expansion and recovery phases (adapted from Kistler et al., 2005).

The inferred half-width of the current sheet and the total plasma pressure are minimal during the interval when O^+ strongly dominates the plasmasheet number and energy densities, with the O^+/H^+ density ratio approaching 10 and the pressure ratio exceeding 10. This extreme situation persists until H^+ starts to replenish at about 0955 UT, perhaps from a dawnside solar wind source, although oxygen continues to dominate the pressure of the plasmasheet during substorm recovery. A similar analysis of a nonstorm–substorm by Kistler et al. (2005) shows that the plasmasheet O^+/H^+ number (<0.4) and energy (<0.9) density ratios never exceed one during the event, but, like the stormtime substorms, both ratios increase after onset, with the largest values achieved after the X-line migrates tailward of the spacecraft. The major difference involves the absolute number densities; the plasmasheet is more tenuous for the nonstorm-substorm described by Kistler et al. For the storm-substorms, $n_H \approx 1/cm^3$ before substorm onset and drops by almost two orders of magnitude after onset, while $n_O \approx 0.1/cm^3$ initially and undergoes a comparatively modest depletion after onset. For the nonstorm–substorm analyzed by Kistler et al., initially $n_H \approx 0.3/cm^3$ and $n_O \approx 0.02/cm^3$; n_H decreases by 1/3 after onset. From this limited sample of data from the polar-orbiting Cluster satellites, one might conclude that the stormtime plasmasheet is denser and contains an order of magnitude more oxygen relative to the nonstorm plasmasheet and becomes almost devoid of H^+ during a storm–substorm. However, complementary statistical results from the ISEE equatorial spacecraft suggest that the plasmasheet density and composition are likely to be very inhomogeneous during such events, with the largest relative abundance of O^+ near GSM $Y \approx 0$ (Lennartsson and Shelley, 1986).

It is not clear exactly why the plasmasheet number density of H^+ decreases more than that of O^+ during a storm–substorm expansion. Perhaps both O^+ and H^+ are severely depleted by the magnetotail collapse and associated earthward injection; however, with the lobes still dominantly filled with O^+, the oxygen starts replenishing almost immediately while the dawnside solar wind supply of H^+ takes longer to reach the satellite. The extreme dropouts in both species shortly after substorm onset add some credibility to this idea.

Möbius et al. (1987) observed that plasmasheet O^+ ions are nonadiabatically accelerated in the magnetotail dipolarizations accompanying substorm expansions, with the increase in O^+ energy exceeding that of H^+ by factors of 2 or more (see also Nosé et al., 2000). This effect is also evident in Fig. 8 starting at 0927 UT. However, the progressive increase in the ratio of O^+/H^+ pressure during substorm expansion in Fig. 8 seems to be due to a progressive decrease in the H^+ pressure relative to the O^+ pressure once the flow remains steadily earthward. The ion energy spectra reported by Kistler et al. suggest that this late expansion-phase decrease in the H^+ pressure is mostly regulated by the decrease in H^+ number density. The O^+ pressure evidently sustains the plasmasheet against the lobe magnetic pressure during the interval of O^+ dominance.

The strongly nonadiabatic energization of O^+ during magnetotail dipolarizations shapes the injections of these ions in the inner magnetotail and is responsible for their rapid acceleration to ring current energies of tens to hundreds of keV (Birn et al., 2004). It is therefore not surprising that the increase in the ratio of O^+/H^+ energy density in the ring current with increasing *Dst* follows the same trend as that of the plasmasheet, as shown in Fig. 9. The increase in plasmasheet O^+ density with *Dst* and the development of a partial ring current associated with plasma injections from the magnetotail may also explain in part why the O^+ number density near the duskside magnetopause on average is a factor of 4 larger than that at the dawnside magnetopause and why significantly more O^+ is found in the duskside magnetosheath than in the dawnside magnetosheath (Bouhram et al., 2005).

The energization of topside auroral ions in downward current regions, such as the mid-latitude, duskside region-2 currents, may provide a direct channel for populating the outer ring current without the ionospheric ions first being processed through the plasmasheet, as occurs for cusp and nightside BPS sources. However, if these outflowing ions never encounter the inductive electric fields of a magnetotail collapse, their characteristic outflow energies of several keV may remain moderate and their contribution to the ring current modest. Wygant et al. (1998) have reported the development of large-scale, stormtime electric fields penetrating into the middle and inner magnetosphere, for durations of an hour or more, with the capacity to inject ring-current ions from $L = 8$ to $L = 2.4$ and to energize the particles to energies of 300 keV. For some storms, these inner magnetospheric

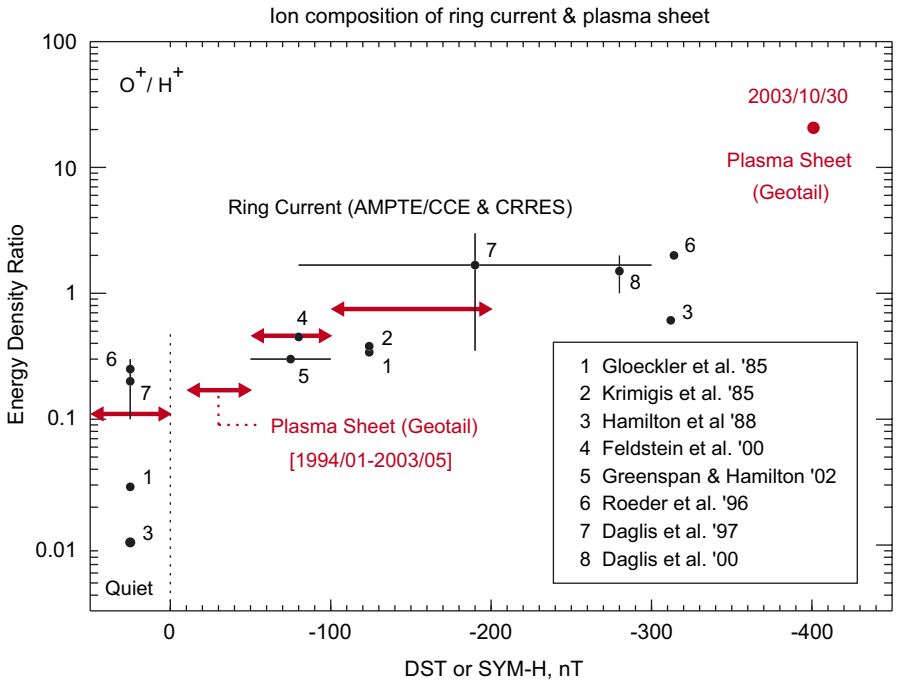

Fig. 9. Ion composition of the ring current and plasmasheet versus *Dst* (from Nosé et al., 2005).

penetrating electric fields may do the job of substorm-induced electric fields.

Large-scale, penetrating electric fields are not fully understood. The ionospheric conductivity appears to play a role in regulating their distribution (Anderson, 2004) and that of the ring current (Liemohn et al., 2005). The observations reported by Wygant et al. of penetrating electric fields in the premidnight sector of the 24 March 1991 storm suggests a possible relation to the partial ring current. The ion pressure associated with the partial ring current leads to stronger duskside Birkeland currents and an asymmetric inflation of the magnetosphere, shifting the ionospheric projection of the currents and their closure through the ionosphere to lower latitudes (Anderson et al., 2005).

5. Impacts on MI coupling

The influence of ionospheric outflow on storm and substorm dynamics has been discussed previously by Daglis and Axford (1996). The models and observations available at that time suggested that an O^+-rich plasmasheet influences the onset of substorm expansion and its tailward location by modifying the stability properties of the plasmasheet, while an O^+-rich ring current supports larger amplitude magnetic storms, with the rapid initial recovery characteristic of great storms attributed to the rapid loss of O^+ ions via charge exchange in the inner ring current. However, an examination (Peterson, 2002) of more recent data and models was unable to affirm or refute the hypothesis that higher abundances of O^+ in the plasmasheet initiate plasma instabilities leading to substorm onset. In addition, if the trend evident in Fig. 9 is a consequence of storm-enhanced O^+ outflows first populating the plasmasheet and inner magnetosphere, and eventually the ring current, then the causality for storms is not entirely clear either: Does an O^+-rich ring current make big storms or do big storms make the ring current O^+-rich?

O^+ dominance of the ring current and the fast charge exchange rate of ~100 keV O^+ relative to H^+ is not the only agent for fast ring-current recovery; for some storms, flow-out loss of the partial ring current to the magnetopause, combined with compositional changes of the plasmasheet source, may account for a substantial part of the initial fast decay of a two-stage recovery (Liemohn et al., 2001). The stormtime ring current clearly involves a dynamic interplay between substorm electric fields, storm-induced penetrating electric fields, variable plasmasheet source densities and

composition, and particle loss mechanisms. Attempts to characterize storm dynamics in terms of a universal paradigm are bound to be disappointing (Daglis et al., 2003).

The presence of oxygen in the velocity shear layer at the magnetopause may enhance flow-out loss there. The observed abundance of ~few keV O^+ ions near the duskside magnetopause lowers the threshold for Kelvin–Helmholtz instability because the increased mass density of the O^+-enriched plasma more closely matches the magnetosheath proton mass density, thereby facilitating the instability's preference for a uniform mass density across the shear layer. The resulting K–H unstable surface waves would presumably enhance plasma transport across the duskside magnetopause. Recent cluster observations and analysis provide convincing evidence for this effect (Bouhram et al., 2005).

An H^+–O^+ admixture in the magnetotail not only has the capacity to modify stability properties, as reviewed by Daglis and Axford (1996), but also the rate and distribution of reconnection. Shay and Swisdak (2004) find that the maximum reconnection outflow in a 2D two-species fluid simulation is about 3 times that in a three-species fluid with $n_O/n_H = 0.64$ and magnetic symmetry representative of the magnetotail. The reconnection rate in the three-species simulation is about 2/3 the rate in the two-fluid plasma. This reconnection rate is either a factor of 2 larger than expected based on the simulated outflow, or the outflow rate is a factor of 2 slower than expected based on the reconnection rate. Given the simulation condition, $m_O n_O \gg m_H n_H$, Shay and Swisdak surmise that the expansion phase of substorms will take longer and will reconnect less lobe magnetic flux in the same amount of time. While the fractional O^+ abundance in the bottom panel of Fig. 8 prior to substorm onset is only about $\frac{1}{2}$ that in the simulation, the simulated abundance condition is well satisfied in the expansion phase in Fig. 8.

What are the system-level implications of these 2D multi-fluid simulation results, if they may be applied to the magnetosphere? One important consequence is an increased demand for episodic unloading of magnetotail flux culminating in substorms of increasing intensity. The slower reconnection rate of an O^+-enriched plasmasheet cannot balance the dayside rate for steady solar wind conditions. This imbalance must be exacerbated with each subsequent substorm, which adds more O^+ to magnetotail. The delivery of interplanetary magnetic flux to the dayside must therefore be dynamically curtailed via some form of feedback that signals the magnetotail's inability to reconnect lobe flux fast enough. Thus far we have no evidence that the dayside abundance of O^+ approaches that of the plasmasheet, so the addition of heavy ions to the dayside is probably insufficient to limit the dayside reconnection efficiency. The maximum stormtime O^+ density reported by Kistler et al. (2005) in the magnetotail is about 4x greater than that at the dayside magnetopause reported by Bouhram et al. (2005).

Global MHD simulations provide some insights into the response of the MI system to this crisis. The force exerted on the magnetosheath flow in its interaction with the dayside region 1 currents is normally weak in comparison with the Chapman–Ferraro currents. However, for the large solar wind electric fields accompanying storms, unusually intense currents are induced by storm-enhanced convection. The global simulations suggest that the magnetic field produced by these currents deflects a portion of the upstream flow and frozen-in magnetic flux before it reaches the magnetopause (Merkine et al., 2003; Siscoe et al., 2004). This purely electrodynamic effect may be further enhanced by the diversion of an O^+-inflated ring current into region-2 currents, most of which must be closed through the ionosphere by the dayside region-1 currents. However, the ring current in the class of one-fluid global simulations considered by Merkine et al. and Siscoe et al. is relatively weak because neither the physics of gradient-curvature drifts nor heavy ion effects are included in the simulations. The simulations include electrodynamic coupling between the magnetosphere and ionosphere but no mass exchange.

Both observations (Russell et al., 2001) and the global simulations reviewed by Siscoe et al. exhibit a nonlinear relationship between the solar wind electric field, $E_{SW} = -v_{SW} \times B_{IMF}$, and the ionospheric transpolar potential (or the cross polar-cap potential). The relationship is linear for $E_{SW} < 5\,\mathrm{mV/m}$. The transpolar potential is observed to nonlinearly saturate at about 200 kV when E_{SW} is greater than about 10 mV/m (Hairston et al., 2005). In the one-fluid global simulations, this saturation is a direct consequence of the interaction between the dayside region-1 currents and the magnetosheath flow.

The cross polar-cap potential is also influenced by the presence of heavy ions in the magnetosphere,

which inertially load the convection. A series of multifluid global simulations of the 24–25 September 1998 magnetic cloud event (minimum $Dst \approx -200$ nT) by Winglee et al. (2002) suggest that O^+ ions may play a major role in limiting the transpolar potential. For the event simulated by Winglee et al., a substantial increase in the observed ionospheric outflow rate caused the mantle to be dominated by plasma of ionospheric origin (Moore et al., 1999). After adjusting the simulated outflow rates to match the statistically observed values for ionospheric O^+ ions reported by Yau and André (1997) and reproduced in Table 1, Winglee et al. found that the simulated potential more closely matched that calculated from the AMIE data assimilation model for the storm event. For lower outflow rates, or outflow without oxygen, the simulated transpolar potential was found to be unrealistically large as shown in Fig. 10. The power dissipated by the accelerated O^+ outflow was also found to be substantial in the simulations, on the order of 100 GW, for sustained southward IMF.

Winglee et al. offer the following explanation for the simulated reduction in the cross-polar cap potential. The momentum flux imparted to the magnetosphere by the solar wind is limited by the "approximately" fixed cross–section of the magnetosphere exposed to the solar wind. If the transfer of solar wind momentum to the magnetosphere is more or less fixed, then a more massive, O^+-enriched magnetosphere on average must convect more slowly than a pure H^+ magnetosphere.

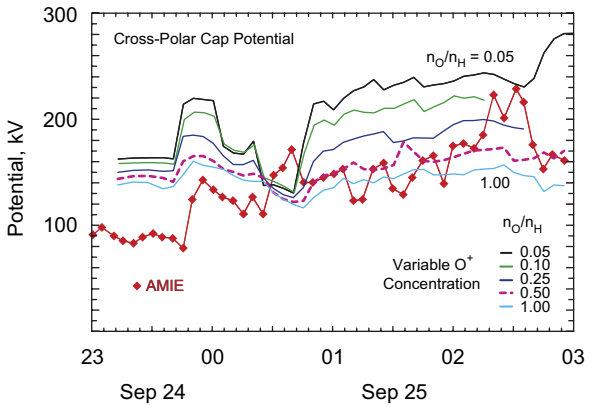

Fig. 10. Cross polar cap potential versus UT during a $Dst \approx -200$ nT storm. The potential derived from the AMIE data assimilation model is compared with results from multifluid global MHD simulations with the indicated O^+ concentrations of the polar wind source specified at the inner simulation boundary (from Winglee et al., 2002).

The convection electric field is thus reduced. Because the transpolar potential is an integral measure of the convection electric field, for a fixed polar cap area it must also decrease with the addition of O^+ to the magnetosphere. However, the area of the polar cap in these simulations decreases with the addition of O^+, so part of the reduction in the transpolar potential may be due to a smaller polar cap size and a smaller magnetospheric cross-section exposed to the solar wind.

The rate at which O^+ is added to the magnetosphere is determined by two different processes in Winglee et al.'s simulation model. The first is the thermal outflow at the inner simulation boundary, which physically resembles a polar wind. The outflowing flux at this boundary is set by gravity, the multifluid densities and temperatures and, therefore, the fixed partial pressures specified at the inner boundary, and the variable relative pressure in the magnetospheric domain which draws plasma from the boundary source. Once in the mantle and polar-cap-lobe region, the outflow experiences the centrifugal acceleration mentioned in Secion 4. The centrifugal force accelerates the outflowing particles along field lines, which enhances their fluxes and energies at high altitudes and establishes the following feedback loop. The centrifugal acceleration depends on the convection electric field. Fast convection gives rise to fast centrifugal acceleration of the thermal outflow, which throttles the lobe-region O^+ flux reaching the magnetotail and the magnetosphere. However, with more O^+ in the magnetospheric circulation system, the convection becomes inertially loaded, which slows the convection and, with it, the centrifugal acceleration, thereby choking the high-altitude flux reaching the magnetotail and the magnetosphere. What is not clear in this picture is how the dynamics of convection and centrifugal acceleration modify the lobe pressure which must regulate the thermal outflow and, therefore, the mass addition at the source boundary.

The electrodynamic effects described by Siscoe et al. (2004) modify the *external* flow and reduce the magnetic flux delivered to the dayside, in contrast with the inertial effects described by Winglee et al. which seem to act entirely internally. It is difficult to compare and assess the relative contributions of electrodynamic and inertial feedback in the two approaches. In one set of models (one-fluid MHD), the ionospheric electrodynamics are a major factor in regulating the solar wind–magnetosphere

coupling, with the solar wind dynamo supplying ~100 GW to ionospheric Joule dissipation; however, the inertial loading associated with ionospheric outflow is completely absent in these models. In the multifluid model of Winglee et al., the ionospheric electrodynamics are passive while ionospheric outflow and centrifugal acceleration of O^+ over the polar cap draw ~100 GW from the solar wind dynamo. A composite model that includes realistic electrodynamic and multispecies inertial coupling between the magnetosphere and ionosphere is clearly needed to resolve these issues.

6. Summary

Convective surges in *F*-region plasma transport give rise to enhanced outflows to the magnetosphere. The ability to image such surges in synoptic TEC-convection maps brings the dynamics of ionospheric plasma redistribution and its implications for dynamic MI coupling clearly into focus.

6.1. O^+ outflows

The most profuse outflows of O^+ occur above the magnetic footpoints of reconnection activity—the low-altitude cusp at the base of magnetopause reconnection and the auroral-polar cap boundary region corresponding to the low-altitude projection of the plasma sheet boundary layer. Large outflows are also found in nightside regions of downward field-aligned current. Alfvén wave activity of different origins is prevalent in all three regions, and the O^+ outflow from each region intersects the equatorial magnetosphere at a different location.

The energy-latitude dispersed outflow from the cusp becomes the cleft ion fountain and mantle at higher altitude and injects a broad swath of tailward flowing plasma into the lobes. The low-altitude cusp region is the ionosphere's most persistent source of outflowing O^+. Mass-independent centrifugal acceleration associated with the convecting field lines threading the mantle boosts the parallel velocities of these ions by a factor of 10–100, rendering them highly field-aligned by the time they penetrate the middle-to-distant plasmasheet.

O^+ outflows from the nightside auroral-polar cap boundary region—the nightside analogue of the cusp—are more intense but also more variable than cusp outflows because the largest fluxes tend to be associated with substorms and other episodic magnetotail activations. These outflows are magnetically connected to the mid-plasmasheet.

Ionospheric ions that reach the magnetotail current sheet are nonadiabatically scattered and accelerated by the cross-tail electric field. Some of these ions are lost to the solar wind in tailward flows. Those that convect earthward into the inner-to-middle plasmasheet are rapidly energized when they encounter substorm-induced electric fields. The magnetotail collapse forces their injection into the near-earth plasmasheet and ring current. O^+ can dominate the plasmasheet density and pressure during the expansion phase of stormtime substorms. However, this dominance is due to an exodus of H^+ from the region rather than an increase in O^+. The ratio of O^+/H^+ energy density of the ring current exhibits a similar trend to that of the plasmasheet during intense storms.

The outflows originating in regions of downward field-aligned current intersect the near-earth plasmasheet, and perhaps the magnetospheric region of the partial ring current. Ordinarily these ions are not boosted to ring-current energies because they do not experience the inductive fields of magnetotail collapse with the same intensity as ions in the plasmasheet. However, when storm-enhanced electric fields penetrate the mid ($L = 8$) to low ($L = 2$) latitude magnetosphere, these ions may be energized to several hundred keV.

The presence of O^+ near the dayside magnetopause lowers the threshold for the Kelvin-Helmholtz instability in the low-latitude boundary layer. The enhanced transport associated with KH turbulence has the capacity to increase the flow-out loss of ring current O^+ at the magnetopause during storm intervals.

6.2. System impacts

Three-fluid simulations suggest that a relatively high O^+ abundance (density ~50% of H^+) slows the reconnection rate by a factor of 2/3 for a magnetic configuration representative of a stressed magnetotail. The global implication of a higher O^+ abundance in the stormtime plasmasheet than in the dayside magnetosphere is an imbalance in the dayside and nightside merging rates. Given that magnetotail reconnection more typically occurs in episodic events such as substorms, these episodes would need to become more frequent or more intense to globally preserve magnetic flux. However,

either outcome would bring even more oxygen into the magnetotail, further exacerbating the imbalance.

This crisis might be moderated in two different and complementary ways. (1) If the intensification and diversion of an O^+-enriched ring current augments the region-2 currents, then closure between the dayside region-2 and region-1 currents through the ionosphere would also augment the region-1 currents. One-fluid global MHD simulations indicate that during intense storms the magnetic field induced by the enhanced dayside region-1 currents deflects a portion of the upstream flow before it reaches the magnetopause, thereby reducing the magnetic flux delivered to the dayside. (2) Multifluid global simulations suggest that inertial loading of the magnetospheric plasma can also significantly reduce convection over the polar cap, thereby reducing the magnetic flux delivered to the magnetotail. In the simulations, a 50/50 O^+/H^+ abundance reduces the transpolar potential by about 50%. Of course, a reduction in flux transport to the nightside must also be accompanied by a corresponding reduction in the dayside merging rate, at least in an average sense, to maintain system balance. Thus both electrodynamic and inertial coupling between solar wind, magnetosphere and ionosphere are crucial elements in the system dynamics.

Acknowledgments

Development of this tutorial has been sponsored by the NASA Heliophysics Theory Program under Grant number NNG05GJ70G, by the Center for Integrated Space Weather Modeling, which is funded by the Science and Technology Centers program of the National Science Foundation under Agreement number ATM-0120950, and by the Thayer School of Engineering at Dartmouth College.

References

Abe, T., Yau, A.W., Watanabe, S., Yamada, M., Sagawa, E., 2004. Long-term variation of the polar wind velocity and its implication for the ion acceleration process: Akebono/suprathermal ion mass spectrometer observations. Journal of Geophysical Research 109, A09305.

Anderson, B.J., Otani, S.-I., Korth, H., Ukhorskiy, A., 2005. Stormtime dawn-dusk asymmetry of the large-scale Birkeland currents. Journal of Geophysical Research 110, A12220.

Anderson, P.C., 2004. Subauroral electric fields and magnetospheric convection during the April, 2002 geomagnetic storms. Geophysical Research Letters 31, L11801.

Andersson, L., Ergun, R.E., Newman, D.L., McFadden, J.P., Carlson, C.W., Su, Y.-H., 2002. Characteristics of parallel electric fields in the downward current region of the aurora. Physics of Plasmas 9 (8), 3600–3609.

Andersson, L., Peterson, W.K., McBryde, K.M., 2005. Estimates of the suprathermal O^+ outflow characteristic energy and relative location in the auroral oval. Geophysical Research Letters 32, L09104.

Atkinson, G., 1970. Auroral arcs: result of the interaction of a dynamic magnetosphere with the ionosphere. Journal of Geophysical Research 75, 4746.

Banks, P.M., Holzer, T.E., 1968. The polar wind. Journal of Geophysical Research 73, 6846–6854.

Birn, J., Thomsen, M.F., Hesse, M., 2004. Acceleration of oxygen ions in the dynamic magnetotail. Annales Geophysicae 22, 1305–1315.

Bouhram, M., Klecker, B., Miyake, W., Rème, H., Sauvaud, J.-A., Malingre, M., Kistler, L., Blăgău, A., 2004. On the altitude dependence of transversely heated O+ distributions in the cusp/cleft. Annales Geophysicae 22, 1787–1798 doi:1432-0576/ag/2004-22-1787.

Bouhram, M., Klecker, B., Paschmann, G., Haaland, S., Hasegawa, H., Blagau, A., Rème, H., Sauvaud, J.-A., Kistler, L.M., Balogh, A., 2005. Survey of energetic O+ ions near the dayside mid-latitude magnetopause with Cluster. Annales Geophysicae 23, 1281–1294.

Cannata, R.W., Gombosi, T.I., 1989. Modeling the solar cycle dependence of quiet-time ion upwelling at geomagnetic latitudes. Geophysical Research Letters 16 (10), 1141–1144.

Carlson, C.W., et al., 1998. FAST observations in the downward auroral current region: Energetic upgoing electron beams, parallel potential drops, and ion heating. Geophysical Research Letters 25, 2017.

Carlson, H.C., Moen, J., Oksavik, K., Nielsen, C.P., McCrea, I.W., Pedersen, T.R., Gallop, P., 2006. Direct observations of injection events of subauroral plasma into the polar cap. Geophysical Research Letters 33, L05103.

Chappell, C.R., Giles, B.L., Moore, T.E., Delcourt, D.C., Craven, P.D., Chandler, M.O., 2000. The adequacy of the ionospheric source in supplying magnetospheric plasma. Journal of Atmospheric and Solar-Terrestrial Physics 62, 421–436.

Chaston, C.C., Bonnell, J.W., Carlson, C.W., McFadden, J.P., Ergun, R.E., Strangeway, R.J., 2003. Properties of small-scale Alfvén waves and accelerated electrons from FAST. Journal of Geophysical Research 108 (A4), 8003.

Chaston, C.C., Bonnell, J.W., Carlson, C.W., McFadden, J.P., Ergun, R.E., Strangeway, R.J., Lund, E.J., 2004. Auroral ion acceleration in dispersive Alfvén waves. Journal of Geophysical Research 109, A04205.

Chaston, C.C., et al., 2005. Energy deposition by Alfvén waves into the dayside auroral oval: Cluster and FAST observations. Journal of Geophysical Research 110, A02211.

Cladis, J.B., 1986. Parallel acceleration and transport of ions from polar ionosphere to plasma sheet. Geophysical Research Letters 13, 893.

Cladis, J.B., Collin, H.L., Lennartsson, O.W., Moore, T.E., Peterson, W.K., Russell, C.T., 2000. Observations of centrifugal acceleration during compression of magnetosphere. Geophysical Research Letters 27, 915–918.

Cully, C.M., Donovan, E.F., Yau, A.W., Arkos, G.G., 2003. Akebono/suprathermal mass spectrometer observations of

low-energy ion outflow: dependence on magnetic activity and solar wind conditions. Journal of Geophysical Research 108 (A2), 1093.

Daglis, I.A., Axford, W.I., 1996. Fast ionospheric response to enhanced activity in geospace: ion feeding of the inner magnetotail. Journal of Geophysical Research 101, 5047–5065.

Daglis, I.A., Kozyra, J.U., Kamide, Y., Vassiliadis, D., Sharma, A.S., Liemohn, M.W., Gonzalez, W.D., Tsurutani, B.T., Lu, G., 2003. Intense space storms: critical issues and open disputes. Journal of Geophysical Research 108 (A5), 1208.

Doe, R.A., Vickrey, J.F., Mendillo, M., 1995. Electrodynamic model for the formation of auroral ionospheric cavities. Journal of Geophysical Research 100 (A6), 9683–9696.

Dombeck, J., Cattell, C., Wygant, J.R., Keiling, A., Scudder, J., 2005. Alfvén waves and Poynting flux observed simultaneously by Polar and FAST in the plasma sheet boundary layer. Journal of Geophysical Research 110, A12S90.

Evans, D.S., Maynard, N., Trøim, J., Jacobsen, T., Egeland, A., 1977. Auroral vector electric field and particle comparisons 2. Electrodynamics of an arc. Journal of Geophysical Research 82 (16), 2235–2249.

Fedder, J.A., Lyon, J.G., 1987. The solar wind–magnetosphere–ionosphere current–voltage relationship. Geophysical Research Letters 14, 880–883.

Foster, J.C., Coster, A.J., Erickson, P.J., Rich, F.J., Sandel, B.R., 2004. Stormtime observations of the flux of plasmaspheric ions to the dayside cusp/magnetopause. Geophysical Research Letters 31, L08809.

Foster, J.C., Coster, A.J., Erickson, P.J., Holt, J.M., Lind, F.D., Rideout, W., McCready, M., van Eyken, A., Barnes, R.J., Greenwald, R.A., Rich, F.J., 2005. Multiradar observations of the polar tongue of ionization. Journal of Geophysical Research 110, A09S31.

Gary, J., Heelis, R., Thayer, J., 1995. Summary of field–aligned Poynting flux observations. Geophysical Research Letters 22, 1861.

Gorney, D.J., Chiu, Y.T., Croley, D.R., 1985. Trapping of ion conics by downward parallel electric fields. Journal of Geophysical Research 90, 4205.

Hairston, M.R., Drake, K.A., Skoug, R., 2005. Saturation of the ionospheric polar cap potential during the October–November 2003 superstorms. Journal of Geophysical Research 110, A09S26.

Huddleston, M.M., Chappell, C.R., Delcourt, D.C., Moore, T.E., Giles, B.L., Chandler, M.O., 2005. An examination of the process and magnitude of ionospheric plasma supply to the magnetosphere. Journal of Geophysical Research 110, A12202.

Hultqvist, B., Øieroset, M., Paschmann, G., Treumann, R. (Eds.), 1999. Magnetospheric Plasma Sources and Losses. Kluwer Academic Publishers, Dordrecht, Boston, London.

Iijima, T., Potemra, T.A., 1976. The amplitude distribution of field-aligned currents at northern high latitudes observed by Triad. Journal of Geophysical Research 81, 2165–2174.

Johnson, R.G. (Ed.), 1983. Energetic Ion Composition in the Earth's Magnetosphere. Terra Scientific Publishing, Tokyo and Reidel Publishing, Dordrecht, Boston, and London.

Kelley, M.C., Vlasov, M.N., Foster, J.C., Coster, A.J., 2004. A quantitative explanation for the phenomenon known as storm-enhanced density. Geophysical Research Letters 31, L19809.

Keiling, A., Wygant, J.R., Cattell, C.A., Mozer, F.S., Russell, C.T., 2003. The global morphology of wave Poynting flux: Powering the aurora. Science 299, 383–386.

Kistler, L.M., Mouikis, C., Möbius, E., Klecker, B., Sauvaud, J.-A., Réme, H., Korth, A., Marcucci, M.F., Lundin, R., Parks, G.K., Balogh, A., 2005. Contribution of nonadiabatic ions to the cross-tail current in an O^+ dominated thin current sheet. Journal of Geophysical Research 110, A06213.

Knudsen, W.C., 1974. Magnetospheric convection and the high-latitude F2 ionosphere. Journal of Geophysical Research 79, 1046.

Knudsen, D.J., Whalen, B.A., Abe, T., Yau, A., 1994. Temporal evolution and spatial dispersion of ion conics: evidence for a polar cusp heating wall. In: Burch, J.L., Waite, J.H. (Eds.), Solar System Plasmas in Space and Time. Geophysical Monograph Series, vol. 84. American Geophysical Union, pp. 163–169.

Lennartsson, O.W., Collin, H.L., Peterson, W.K., 2004. Solar wind control of Earth's H^+ and O^+ outflow rates in the 15-eV to 33-keV energy range. Journal of Geophysical Research 109, A12212.

Lennartsson, O.W., Sharp, R.D., 1982. A comparison of the 0.1–17 keV/e ion composition in the near equatorial magnetosphere between quiet and disturbed conditions. Journal of Geophysical Research 87 (A8), 6109–6120.

Lennartsson, O.W., Shelley, E.G., 1986. Survey of 0.1- to 16-kev/e plasma sheet ion composition. Journal of Geophysical Research 91 (A3), 3061–3076.

Liemohn, M.W., Kozyra, J.U., Thomsen, M.F., Roeder, J.L., Lu, G., Borovsky, J.E., Cayton, T.E., 2001. Dominant role of the asymmetric ring current in producing the stormtime *Dst**. Journal of Geophysical Research 106, 10883–10904.

Liemohn, M.W., Ridley, A.J., Brandt, P.C., Gallagher, D.L., Kozyra, J.U., Ober, D.M., Mitchell, D.G., Roelof, E.C., DeMajistre, R., 2005. Parametric analysis of nightside conductance effects on inner magnetospheric dynamics for the 17 April 2002 storm. Journal of Geophysical Research 110, A12S22.

Liu, C., Horwitz, J.L., Richards, P.G., 1995. Effects of frictional ion heating and soft-electron precipitation on high-latitude F-region upflows. Geophysical Research Letters 22, 2713–2716.

Lockwood, M., Chandler, M.O., Horwitz, J.L., Waite Jr., J.H., Moore, T.E., Chappell, C.R., 1985. The cleft ion fountain. Journal of Geophysical Research 90, 9736–9748.

Lund, E.J., Möbius, E., Carlson, C.W., Ergun, R.E., Kistler, L.M., Klecker, B., Klumpar, D.M., McFadden, J.P., Popecki, M.A., Strangeway, R.J., Tung, Y.K., 2000. Transverse ion acceleration mechanism in the aurora at solar minimum: occurrence distributions. Journal of Atmospheric and Solar-Terrestrial Physics 62, 467–475.

Lynch, K.A., Bonnell, J.W., Carlson, C.W., Peria, W.J., 2002. Return current region aurora: $E_{||}$, j_z, particle energization, and broadband ELF wave activity. Journal of Geophysical Research 107 (A7), 1115.

Lysak, R.L., Song, Y., 2002. Energetics of the ionospheric feedback interaction. Journal of Geophysical Research 107 (A8), 1160.

Merkine, V.G., Papadopoulos, K., Milikh, G., Sharma, A.S., Shao, X., Lyon, J., Goodrich, C., 2003. Effects of the solar wind electric field and ionospheric conductance on the cross polar cap potential: results of global MHD modeling. Geophysical Research Letters 30 (23), 2180.

Möbius, E., Scholer, M., Klecker, B., Hovestadt, D., Gloeckler, G., Ipavich, F.M., 1987. Acceleration of ions of ionospheric origin in the plasma sheet during substorm activity. In: Liu, A.T.Y. (Ed.), Magnetotail Physics. Johns Hopkins Univ. Press, Baltimore, Md., pp. 231–234.

Moore, T.E., Peterson, W.K., Russell, C.T., Chandler, M.O., Collier, M.R., Collin, H.L., Craven, P.D., Fitzenreiter, R., Giles, B.L., Pollock, C.J., 1999. Ionospheric mass ejection in response to a CME. Geophysical Research Letters 26, 2339.

Nilsson, H., et al., 2006. Characteristics of high altitude oxygen ion energization and outflow as observed by Cluster: a statistical study. Annales Geophysicae 24, 1099–1112.

Nosé, M., Ohtani, S., Lui, A.T.Y., Chaston, S.P., McEntire, R.W., Williams, D.J., Mukai, T., Saito, Y., Yumoto, K., 2000. Change of energetic ion composition in the plasma sheet during substorms. Journal of Geophysical Research 105 (A10), 23277–23286.

Nosé, M., Taguchi, S., Hosokawa, K., Christon, S.P., McEntire, R.W., Moore, T.E., Collier, M.R., 2005. Overwhelming O^+ contribution to the plasma sheet energy density during the October 2003 superstorm: Geotail/EPIC and IMAGE/LENA observations. Journal of Geophysical Research 110, A09S24.

Ober, D.M., Maynard, N.C., Burke, W.J., 2003. Testing the Hill model of transpolar saturation. Journal of Geophysical Research 108 (A12), 1467.

Olsson, A., Janhunen, P., Karlsson, T., Ivchenko, N., Blomberg, L.G., 2004. Statistics of Joule heating in the auroral zone and polar cap using Astrid-2 satellite Poynting flux. Annales Geophysicae 22, 4133–4142.

Paschmann, G., Haaland, S., Treumann, R. (Eds.), 2003. Auroral Plasma Physics. Kluwer Academic Publishers, Boston/Dordrecht/London.

Peterson, W.K., 2002. Ionospheric influence on substorm development. In: Winglee, R.M. (Ed.), Proceedings of the 6th International Conference on Substorms (ICS-6). University of Washington, Seattle, pp. 143–150.

Peterson, W.K., Sharp, R.D., Shelley, E.G., Johnson, R.G., Balsinger, H., 1981. Energetic ion composition of the plasma sheet. Journal of Geophysical Research 86, 761.

Peterson, W.K., Collin, H.L., Yau, A.W., Lennartsson, O.W., 2001. Polar/Toroidal imaging mass-angle spectrograph observations of suprathermal ion outflow during solar minimum conditions. Journal of Geophysical Research 106 (A4), 6059–6066.

Peterson, W.K., Collin, H.L., Lennartsson, O.W., Yau, A.W., 2006. Quiet time solar illumination effects on the fluxes and characteristic energies of ionospheric outflow. Journal of Geophysical Research 111, A11S05.

Pokhotelov, D., Lotko, W., Streltsov, A.V., 2002. Harmonic structure of field line eigenmodes generated by ionospheric feedback instability. Journal of Geophysical Research 107 (A11), 1363.

Reiff, P.H., Luhmann, J.G., 1986. Solar wind control of the polar cap potential. In: Kamide, Y., Slavin, J.A. (Eds.), Solar Wind-Magnetospheric Coupling. Terra Scientific, Tokyo, p. 453.

Russell, C.T., Luhmann, J.G., Lu, G., 2001. Nonlinear response of the polar ionosphere to large values of the interplanetary electric field. Journal of Geophysical Research 106 (A9), 18,495–18,504.

Sato, T., 1959. Morphology of ionospheric F2 disturbances in the polar regions: a linkage between polar patches and plasmaspheric drainage plumes. Reports on Ionospheric Research and Space Research of Japan 13, 91.

Sato, T., 1978. A theory of quiet auroral arcs. Journal of Geophysical Research 83, 1042.

Sauvaud, J.-A., et al., 2004. Case studies of the dynamics of ionospheric ions in the Earth's magnetotail. Journal of Geophysical Research 109, A01212.

Schunk, R.W., Sojka, J.J., 1997. Global ionosphere-polar wind system during changing magnetic activity. Journal of Geophysical Research 102, 11,625–11,651.

Schunk, R.W., Demars, H.G., Sojka, J.J., 2005. Propagating polar wind jets. Journal of Atmospheric and Solar-Terrestrial Physics 67, 357–364.

Shelley, E.G., Collin, H.L., 1991. Auroral ion acceleration and its relationship to ion composition. In: Meng, C.-I., Rycroft, M.J., Frank, L.J. (Eds.), Auroral Physics. Cambridge University Press, New York, p. 129.

Seki, K., Hirahara, M., Terasawa, T., Mukai, T., Saito, Y., Machida, S., Yamamoto, Y., Kokubun, S., 1998. Statistical properties and possible supply mechanism of tailward cold O^+ beams in the lobe/mantle regions. Journal of Geophysical Research 103, 4477.

Semeter, J., Heinselman, C.J., Thayer, J.P., Frey, H.U., 2003. Ion upflow enhanced by drifting F-region plasma structure along the nightside polar cap boundary. Geophysical Research Letters 30 (22), 2139.

Sharp, R.D., Carr, D.L., Peterson, W.K., Shelley, E.G., 1981. Ion streams in the magnetotail. Journal of Geophysical Research 86 (A6), 4639–4648.

Shay, M.A., Swisdak, M., 2004. Three-species collisionless reconnection: effect of O^+ on magnetotail reconnection. Physical Review Letters 93 (17), 175001(4).

Siscoe, G.L., Raeder, J., Ridley, A.J., 2004. Transpolar potential saturation models compared. Journal of Geophysical Research 109, A09203.

Sojka, J.J., Bowline, M.D., Schunk, R.W., Decker, D.T., Valladares, C.E., Sheehan, R., Anderson, D.A., Heelis, R.A., 1993. Modeling polar cap F-region patches using time varying convection. Geophysical Research Letters 20, 1783.

Sojka, J.J., Subramanium, M.V., Zhu, L., Schunk, R.W., 1998. Gradient-drift instability growth rates from global scale modeling of the polar ionosphere. Radio Sci 33 (6), 1915–1928.

Strangeway, R.J., Ergun, R.E., Su, Y.-J., Carlson, C.W., Elphic, R.C., 2005. Factors controlling ionospheric outflows as observed at intermediate altitudes. Journal of Geophysical Research 110, A03221.

Streltsov, A.V., Lotko, W., 2003. Small-scale electric fields in downward auroral current channels. Journal of Geophysical Research 108 (A7), 1289.

Streltsov, A.V., Lotko, W., 2004. Multiscale electrodynamics of the ionosphere-magnetosphere system. Journal of Geophysical Research 109, A09214.

Tung, Y.-K., Carlson, C.W., McFadden, J.P., Klumpar, D.M., Parks, G.K., Peria, W.J., Liou, K., 2001. Auroral polar cap boundary ion conic outflow observed on FAST. Journal of Geophysical Research 106 (A3), 3603–3614.

Valek, P.W., Perez, J.D., Jahn, J.-M., Pollock, C.J., Wüest, M.P., Friedel, R.H.W., Moore, T.E., Peterson, W.K., 2002. Outflow from the ionosphere in the vicinity of the cusp. Journal of Geophysical Research 10 (A8), 1180.

Winglee, R.M., Chua, D., Brittnacher, M., Parks, G.K., Lu, G., 2002. Global impact of ionospheric outflows on the dynamics of the magnetosphere and cross-polar cap potential. Journal of Geophysical Research 107 (A9), 1237.

Yau, A.W., André, M., 1997. Source of ion outflow in the high latitude ionosphere. Space Science Review 80, 1.

Zheng, Y., Moore, T.E., Mozer, F.S., Russell, C.T., Strangeway, R.J., 2005. Polar study of ionospheric ion outflow versus energy input. Journal of Geophysical Research 110, A07210.